8-2016

Active Fault Tolerant Control for Vertical Tail Damaged Aircraft with Dissimilar Redundant Actuation System

Wang Jun

Wang Shaoping

Wang Xingjian

Shi Cun

Mileta M. Tomovic
Old Dominion University, mtomovic@odu.edu

Original Publication Citation

Wang, J., Wang, S., Wang, X., Shi, C., & Tomovic, M. M. (2016). Active fault tolerant control for vertical tail damaged aircraft with dissimilar redundant actuation system. *Chinese Journal of Aeronautics, 29*(5), 1313-1325. doi:10.1016/j.cja.2016.08.009

Chinese Journal of Aeronautics, (2016), 29(5): 1313–1325

Chinese Society of Aeronautics and Astronautics
& Beihang University

Chinese Journal of Aeronautics

cja@buaa.edu.cn
www.sciencedirect.com

Active fault tolerant control for vertical tail damaged aircraft with dissimilar redundant actuation system

Wang Jun [a], **Wang Shaoping** [a], **Wang Xingjian** [a,*], **Shi Cun** [a], **Mileta M. Tomovic** [b]

[a] *School of Automation Science and Electrical Engineering, Beihang University, Beijing 100083, China*
[b] *College of Engineering and Technology, Old Dominion University, Norfolk, VA 23529, USA*

Received 13 October 2015; revised 28 March 2016; accepted 13 May 2016
Available online 27 August 2016

KEYWORDS

Dissimilar redundant actuation system;
Electro-hydrostatic actuator;
Fault-tolerant control;
Linear quadratic regulator;
Model reference adaptive control;
Nonlinear aircraft model;
Vertical tail loss

Abstract This paper proposes an active fault-tolerant control strategy for an aircraft with dissimilar redundant actuation system (DRAS) that has suffered from vertical tail damage. A damage degree coefficient based on the effective vertical tail area is introduced to parameterize the damaged flight dynamic model. The nonlinear relationship between the damage degree coefficient and the corresponding stability derivatives is considered. Furthermore, the performance degradation of new input channel with electro-hydrostatic actuator (EHA) is also taken into account in the damaged flight dynamic model. Based on the accurate damaged flight dynamic model, a composite method of linear quadratic regulator (LQR) integrating model reference adaptive control (MRAC) is proposed to reconfigure the fault-tolerant control law. The numerical simulation results validate the effectiveness of the proposed fault-tolerant control strategy with accurate flight dynamic model. The results also indicate that aircraft with DRAS has better fault-tolerant control ability than the traditional ones when the vertical tail suffers from serious damage.

1. Introduction

Structural damage to an aircraft, like the damage/loss of a vertical tail, can lead to loss of controllability, which would create a challenging situation for the pilots.[1–3] An example of such a situation, is the disaster that involved the Boeing 747 freighter aircraft that crashed in Mount Osutaka in 1985, with no one survived (520 fatalities). In this particular case, the aircraft lost the vertical tail and the hydraulic pipelines were pulled apart. This damage caused significant loss of controllability and, next to that, structural changes, which led to the crash. Another such similar example was 2001-A300, vertical tail loss, 265 fatalities. Such failures were likely to be survivable, if given correct control input and a wise trajectory. However, there were no effective measures for these aircraft with traditional centralized hydraulic actuation system (HAS) in such extreme situations, since the vertical tail loss would pull apart the hydraulic

* Corresponding author. Tel.: +86 10 82338917.
E-mail addresses: dwill-wang@buaa.edu.cn (J. Wang), shaoping-wang@vip.sina.com (S. Wang), wangxj@buaa.edu.cn (X. Wang), shicun@buaa.edu.cn (C. Shi), mtomovic@odu.edu (M.M. Tomovic).
Peer review under responsibility of Editorial Committee of CJA.

Production and hosting by Elsevier

http://dx.doi.org/10.1016/j.cja.2016.08.009
1000-9361

pipelines and lead the aircraft to lose pressures to actuate. Fortunately, the modern civil aircraft are developing toward the trend of being powered electrically more and more. Electro-hydrostatic actuators (EHA) have been applied in aircraft together with traditional centralized HAS, which produces dissimilar redundant actuation system (DRAS).[4,5] Consequently, there has been a growing interest in new-type aircraft with this kind of new actuation system. The commercial aircraft, A380, A350 and A400M of Airbus Company have adopted DRAS of 2H/2E type. Researches about DRAS are being done as one effective measure to further enhance the flight safety.[6] These researches indicate that aircraft with DRAS have potential fault-tolerant capability to respond to some extreme situations. Therefore, it is desirable to develop fault-tolerant mechanisms for aircraft with DRAS that can assist the crew in some severe situations.

Outer mold line changes due to the damage can result in nonlinear and/or non-symmetric mass properties, aerodynamics, or control characteristics.[7] Though it is difficult to analytically estimate or predict such characteristics or their impact, it is still very necessary to study the relationship between the damage degree and the dynamic model to service the fault-tolerant control (FTC) strategy design. The general effects of vertical tail damage on directional characteristics are similar in nature to those seen in the pitch axis from stabilizer damage, namely, a reduction in static and dynamic stability. Much earlier work has been done to study the damaged aircraft modeling and the fault-tolerant strategy.[8–10] In these researches, the researchers studied the damaged aircraft model with vertical tail loss with not very serious damage using Boeing-747 100/200 data and regarded the input channel can continue to work. However, it is highly possible for the aircraft only with centralized HAS to lose the input channel when suffering from serious vertical tail loss. Besides, in these researches, the damage-induced aerodynamics characteristics change is expressed as a linear scale of the maximum damage degree, the accurate nonlinear relationship between the damage degree and its corresponding stability and control derivatives has not been studied.

For the research about vertical tail loss,[10] since the researchers studied the not very serious damage degree, three passive fault-tolerant control (PFTC) methods: quadratic stabilization, guaranteed cost control and quadratic cost control with robust pole placement were compared. The conclusion is that guaranteed cost control with robust pole placement can have a better control performance when the damage is less than 10%. However, when the damage degree exceeds a critical number, those PFTC methods would be no longer applicable. An active fault-tolerant control (AFTC)[11–15] method should be chosen to respond to extreme situations. Many researchers developed effective control methods to cope with FTC problems of complex system. In Li and Yang's latest research work,[16] an adaptive fuzzy decentralized control method was used to solve the FTC problem of large-scale nonlinear systems with actuator faults and unknown dead zone; in their another work,[17] a robust fuzzy adaptive control method was used to solve the FTC problem of large-scale nonlinear systems with mismatched uncertainties and actuator faults. Both researches indicate the effectiveness of adaptive technique as one important factor of the control method. To compensate for the serious failures of aircraft, Stengel and Huang studied reconfigurable control using proportional-integral implicit model following method very early.[18] Bodson and Groszkiewicz developed a multivariable adaptive algorithm for reconfigurable flight control system.[19] Boškovic and Mehra developed an adaptive control method for a tailless advanced fighter aircraft under wing damage.[20] The later researches, e.g. in Lavretsky's research, an composite model reference adaptive control (MRAC) method was developed by integrating the classical model following method and adaptive control.[21] These researches indicate that MRAC can be an effective FTC method and it is necessary to highlight that in flight control system the determination of control law parameters should be more efficient.

This paper studies the civil aircraft with DRAS and focuses on the modeling of damaged aircraft in vertical tail loss situation and developing FTC strategy. A damage degree coefficient based on the effective vertical tail area is introduced, and then the nonlinear relationship between the damage degree and its corresponding stability and control derivatives are studied. In this way, a flight dynamic model for a damaged aircraft is developed to account for various damage degrees that result in changes to aerodynamics. Furthermore, even the hydraulic systems lose pressure when the pipelines are pulled apart due to vertical tail loss, EHA can continue to actuate to stabilize the dynamic model. Therefore, the performance of EHA is also modeled in the dynamic model. Based on the accurate modeling, an AFTC strategy, using MRAC composed of linear quadratic regulator (LQR) technique,[22,23] is developed. In this way, the control law parameters can be determined by LQR method while the fault-tolerance can be guaranteed by MRAC method. Simulation results illustrate the necessity of accurate modeling and effectiveness of designed FTC strategy.

2. Modeling of damaged aircraft

It is a standard practice to linearize the model around a certain steady flight operating point. When the aircraft suffers from vertical tail damage, only some lateral-directional parameters change, therefore, only the lateral-directional model of the aircraft was considered in this paper. Using the early research work,[10,24] the aircraft model under normal conditions can be represented as follows:

$$\begin{cases} \dot{\boldsymbol{x}} = \boldsymbol{A}\boldsymbol{x} + \boldsymbol{B}\boldsymbol{u}_{\mathrm{H}} \\ \boldsymbol{y} = \boldsymbol{C}\boldsymbol{x} \end{cases} \tag{1}$$

where the state variable vector $\boldsymbol{x} = [\beta, \quad p, \quad r, \quad \phi]^{\mathrm{T}}$, in which β is the sideslip angle, p the roll rate, r the yaw rate, and ϕ the roll angle; the system corresponding matrices are

$$\begin{cases} \boldsymbol{A} = \begin{bmatrix} \frac{Y_\beta}{m} & \frac{Y_p}{m} & \frac{Y_r}{m} - u_0 & g_0 \cos\theta_0 \\ \frac{L_\beta}{I'_x} + I'_{zx} N_\beta & \frac{L_p}{I'_x} + I'_{zx} N_p & \frac{L_r}{I'_x} + I'_{zx} N_r & 0 \\ \frac{N_\beta}{I'_z} + I'_{zx} L_\beta & \frac{N_p}{I'_z} + I'_{zx} L_p & \frac{N_r}{I'_z} + I'_{zx} L_r & 0 \\ 0 & 1 & \tan\theta_0 & 0 \end{bmatrix} \\ \boldsymbol{B} = \begin{bmatrix} \frac{Y_{\delta_\mathrm{a}}}{m} & \frac{Y_{\delta_\mathrm{r}}}{m} \\ \frac{L_{\delta_\mathrm{a}}}{I'_x} + I'_{zx} N_{\delta_\mathrm{a}} & \frac{L_{\delta_\mathrm{r}}}{I'_x} + I'_{zx} N_{\delta_\mathrm{r}} \\ \frac{N_{\delta_\mathrm{a}}}{I'_z} + I'_{zx} L_{\delta_\mathrm{a}} & \frac{N_{\delta_\mathrm{r}}}{I'_z} + I'_{zx} L_{\delta_\mathrm{r}} \\ 0 & 0 \end{bmatrix} \\ \boldsymbol{C} = \begin{bmatrix} 0 & 0 & 0 & 1 \\ 1 & 0 & 0 & 0 \end{bmatrix} \end{cases}$$

For the system matrices, the nomenclature for all the parameters in matrices $\boldsymbol{A}$ and $\boldsymbol{B}$ is the same as in Li and Liu's research work.[10] Where $I'_x = (I_x I_z - I_{zx}^2)/I_z$, $I'_z = (I_x I_z - I_{zx}^2)/I_x$, $I'_{zx} = I_{zx}/(I_x I_z - I_{zx}^2)$; I_x and I_z are inertia moments about (x, z) axes respectively; I_{zx} is the inertia product due to (x, z) axes; Y_β, Y_p and Y_r are the side aerodynamic forces in three stability axes respectively; L_β, L_p and L_r are the rolling moments in three stability axes respectively; N_β, N_p and N_r are the yawing moments in three stability axes respectively; Y_{δ_a} and Y_{δ_r} are side aerodynamic forces provided by ailerons and rudders respectively; L_{δ_a} and L_{δ_r} are the rolling moments provided by ailerons and rudders respectively; N_{δ_a} and N_{δ_r} are the yawing moments provided by ailerons and rudders respectively; m is the total mass of the airplane; u_0 is the reference flight speed; θ_0 is the reference angle of climb; g_0 is the acceleration due to gravity.

$\boldsymbol{u}_H = [\,\delta_a, \quad \delta_r\,]^T$ is the control input vector, and δ_a the control input provided by ailerons, δ_r the control input provided by rudders. The output matrix $\boldsymbol{C}$ indicates that sideslip angle β and roll angle ϕ are the system output.

In this section, the aircraft dynamic model has been well developed. An accurate model can be obtained by considering the nonlinear damage of vertical tail and the performance degradation of EHA.

2.1. Modeling of nonlinear damage

2.1.1. Modeling of vertical tail damage

For aircraft suffering from vertical tail damage, as shown in Fig. 1, the fracture shape caused by vertical tail loss is irregular and some relative assumptions are made for the proceeding of the research.

Assumption 1. The vertical tail shape is regular trapezium and the loss part of vertical tail is equivalent to regular trapezium.

Based on Assumption 1, a parameter μ is introduced to define the damage degree.

Definition 1. Vertical tail damage coefficient μ: the ratio of lost effective area in all effective areas of the vertical tail.

With the above definition, $\mu \in [0, 1]$ can be used to represent different damage cases, especially, $\mu = 0$ represents that the flight model is in normal condition without damage. In order to obtain the nonlinear relationship between μ and all the corresponding stability derivative deviation, the fundamental equation of vertical tail derivative in Eq. (2) is used as

$$C_{y_\beta} = \frac{2\pi A\left(\frac{S_{out}}{S_{ref}}\right)F}{2 + \sqrt{4 + \frac{A^2\beta^2}{\eta^2}\left(1 + \frac{\tan^2 \Lambda_{max\_t}}{\beta^2}\right)}} \tag{2}$$

where C_{y_β} is the damaged vertical tail derivative; $\beta^2 = 1 - Ma^2$, $F = 1.07(1 + d/b)^2$, with Ma the Mach number, b the height of vertical tail and d the fuselage diameter; S_{out} and S_{ref} are exposed area and reference area respectively; $A = b^2/S_{ref}$ is the aspect ratio of vertical tail; Λ_{max_t} is the vertical tail sweep of string position of airfoil thickness; and η is the efficiency of airfoil.

Based on Assumption 1 and Definition 1, several geometric parameters in the case of vertical tail partial loss can be obtained. As shown in Fig. 2, c_t and c_r are the vertical tail tip chord length and the vertical tail root chord length respectively. The exposed area of vertical tail can be obtained as that in Eq. (3).

$$S_{out} = \frac{1}{2}(c_t + c_r)b \tag{3}$$

When the vertical tail damage degree is μ, the vertical tail tip chord length changes from c_t to $c_t(\mu)$; meanwhile, the height of vertical tail deduces by $b(\mu)$, also the aspect ratio of vertical tail changes into $A(\mu)$; considering all these factors, the nonlinear relationship between μ and C_{y_β} can be obtained based on trapezoid area equation. As shown in Fig. 2, the lost area of vertical tail can be represented as

$$\mu S_{out} = \frac{1}{2}(c_t + c_t(\mu))b(\mu) \tag{4}$$

and the rest area of the vertical tail should be

$$(1 - \mu)S_{out} = \frac{1}{2}(c_r + c_t(\mu))(b - b(\mu)) \tag{5}$$

Combining Eqs. (3) and (4), $b(\mu)$ can be obtained as $b(\mu) = \frac{(c_t + c_r)\mu}{c_t + c_t(\mu)}b$, then the effective rest vertical tail height can be represented as

$$b_{left} = b - b(\mu) = b\left[1 - \frac{(c_t + c_r)\mu}{c_t + c_t(\mu)}\right] \tag{6}$$

Combining Eqs. (5) and (6), the representation of the vertical tail tip chord length can be obtained as

$$c_t(\mu) = \sqrt{\frac{2(1 - \mu)c_t + 2\mu c_r}{b}S_{out} - c_t c_r} \tag{7}$$

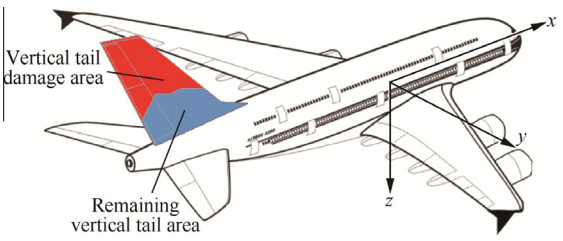

Fig. 1 An aircraft with irregular partial vertical tail loss.

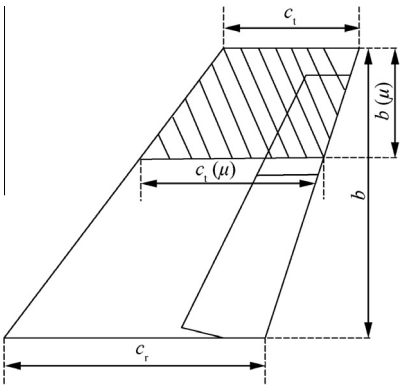

Fig. 2 Regular damage and relative parameters of vertical tail loss.

Then the aspect ratio of vertical tail when the vertical tail suffers from μ degree damage can be obtained as

$$A(\mu)=\frac{b_{\text{left}}^2}{S_{\text{ref}}-S_{\text{out}}+S_{\text{out}}(1-\mu)} \tag{8}$$

Finally the nonlinear relationship between μ and C_{y_β} can be obtained using the above equations as

$$C_{y_\beta}(\mu)=\frac{2\pi A(\mu)\left[\frac{S_{\text{out}}(1-\mu)}{(S_{\text{ref}}-S_{\text{out}})+S_{\text{out}}(1-\mu)}\right]\times 1.07\left(1+\frac{d}{b_{\text{left}}}\right)^2}{2+\sqrt{4+\frac{A^2(\mu)\beta^2}{\eta^2}\left(1+\frac{\tan^2\Lambda_{\max\_t}}{\beta^2}\right)}} \tag{9}$$

In order to simulate the nonlinear relationship between μ and C_{y_β}, this paper uses vertical tail characteristics of Boeing-747 and its corresponding parameters are chosen as: $S_{\text{out}}=77\ \text{m}^2$, $S_{\text{ref}}=87\ \text{m}^2$, $\beta=\pi/16$, $d=6.5$ m, $b=9.8$ m, $\Lambda_{\max\_t}=40^\circ$, $\eta=0.95$, $c_t=4$ m, $c_r=11.7$ m.

The relationship between μ and C_{y_β} is shown in Fig. 3, in which C_{y_β} decreases gradually to 0 as μ changes from 0 to 1. In this process, the relationship between μ and C_{y_β} presents strong nonlinearity. The absolute difference $|\Delta C_{y_\beta}|$ vs μ is shown in Fig. 4, in which $|\Delta C_{y_\beta}|$ reaches the maximum value when the damage degree $\mu=0.9$. Based on this nonlinear function about μ and C_{y_β}, one more precise vertical tail damaged aircraft model can be obtained.

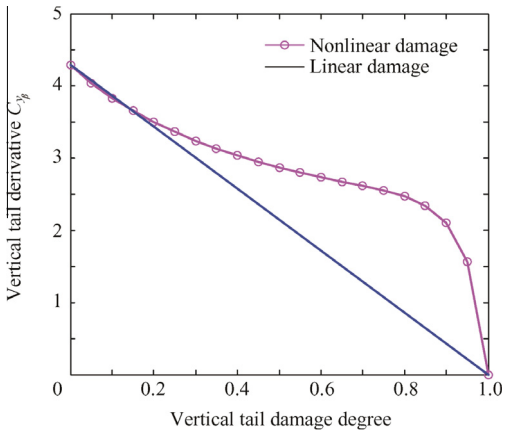

Fig. 3 Function relationship between C_{y_β} and μ.

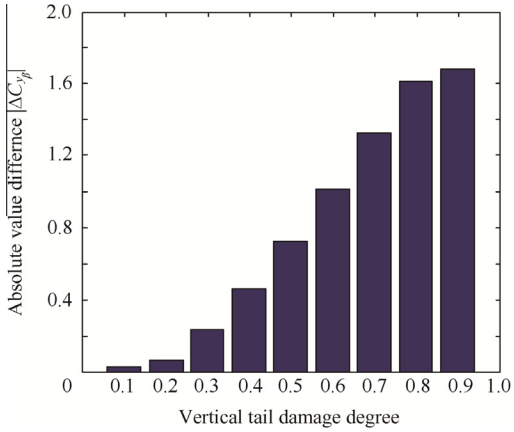

Fig. 4 Absolute value difference of $|\Delta C_{y_\beta}|$ vs μ.

2.1.2. Corresponding dimensional aerodynamic derivatives

In the case of aircraft suffering from vertical tail damage, there are also other damage-induced stability and control derivatives. Using Hitachi's research results,[8] the relationships between $C_{y_\beta}(\mu)$ and the rest corresponding derivatives can be obtained as

$$\begin{cases}
C_{n_\beta}(\mu)=\left[-\left(\frac{l_v}{b_w}\cos\alpha+\frac{z_v}{b_w}\sin\alpha\right)\right]C_{y_\beta}(\mu)\\
C_{l_\beta}(\mu)=\left(\frac{z_v}{b_w}\cos\alpha+\frac{l_v}{b_w}\sin\alpha\right)C_{y_\beta}(\mu)\\
C_{y_p}(\mu)=\left[2\left(\frac{z_v}{b_w}\cos\alpha-\frac{l_v}{b_w}\sin\alpha\right)\right]C_{y_\beta}(\mu)\\
C_{n_p}(\mu)=\left[-\frac{2}{b_w^2}(l_v\cos\alpha+z_v\sin\alpha)(z_v\cos\alpha-l_v\sin\alpha)\right]C_{y_\beta}(\mu)\\
C_{l_p}(\mu)=2\left(\frac{z_v}{b_w}\right)^2C_{y_\beta}(\mu)\\
C_{y_r}(\mu)=\left[-\frac{2}{b_w}(l_v\cos\alpha+z_v\sin\alpha)\right]C_{y_\beta}(\mu)\\
C_{n_r}(\mu)=\left[\frac{2}{b_w^2}(l_v\cos\alpha+z_v\sin\alpha)^2\right]C_{y_\beta}(\mu)\\
C_{l_r}(\mu)=\left[-\frac{2}{b_w^2}(l_v\cos\alpha+z_v\sin\alpha)(z_v\cos\alpha-l_v\sin\alpha)\right]C_{y_\beta}(\mu)
\end{cases} \tag{10}$$

The nomenclature for all the parameters in Eq. (10) and the following Eq. (11) is the same as in Hitachi's research results.[8] Where $C_{n_\beta}(\mu)$ is the weathercock stability derivative; $C_{l_\beta}(\mu)$ is the dihedral effect; $C_{y_p}(\mu)$ is the side force-in-roll derivative, $C_{n_p}(\mu)$ is the cross derivative of rolling-caused yawing moment; $C_{l_p}(\mu)$ is the damping-in-roll derivative; $C_{y_r}(\mu)$ is the attack angle-caused derivative; $C_{n_r}(\mu)$ is the damping-in-yaw derivative; $C_{l_r}(\mu)$ is the cross derivative of yawing-caused rolling moment; b_w is the wing span; l_v and z_v are horizontal and vertical location of the aerodynamic center of the vertical tail; α is the attack angle of the zero lift line.

The affected stability and control derivatives indicate that the vertical tail damage would have significant impact on lateral and directional dynamic behavior. The corresponding changing aerodynamic derivatives in the lateral and directional dynamic model are listed as

$$\begin{cases}
Y_\beta(\mu)=\frac{1}{2}\rho S_w C_{y_\beta}(\mu)\\
Y_r(\mu)=\frac{1}{4}\rho b_w S_w C_{y_r}(\mu)\\
Y_p(\mu)=\frac{1}{4}\rho b_w S_w C_{y_p}(\mu)\\
L_\beta(\mu)=\frac{1}{2}\rho b_w S_w C_{l_\beta}(\mu)\\
L_r(\mu)=\frac{1}{4}\rho b_w^2 S_w C_{l_r}(\mu)\\
L_p(\mu)=\frac{1}{4}\rho b_w^2 S_w C_{l_p}(\mu)\\
N_\beta(\mu)=\frac{1}{2}\rho b_w^2 S_w C_{n_\beta}(\mu)\\
N_r(\mu)=\frac{1}{4}\rho b_w^2 S_w C_{n_r}(\mu)\\
N_p(\mu)=\frac{1}{4}\rho b_w^2 S_w C_{n_p}(\mu)
\end{cases} \tag{11}$$

where ρ is the air density; S_w is the wing reference area.

2.2. Design of performance degradation input function

In this research, the civil aircraft with DRAS was studied. The structure of DRAS is shown in Fig. 5, where u_h and u_e are the input signals for HA and EHA respectively, i_v the electrical signal for the servo valve, and θ_d the deflection angle of the control surface. When the vertical tail suffers from serious damage, the vertical tail loss will pull apart the hydraulic pipelines, and the

whole hydraulic system will lose pressure. In this case, all control surfaces actuated by HA system would be in loose floating state, and then a catastrophic consequence may occur. Fortunately, if the new-type civil aircraft with DRAS can launch EHA to actuate some main control surfaces quickly, the aircraft can survive using this new type actuation system.

HA and EHA are different in response performance. EHA responds more slowly than HA. Therefore, the response performance degradation of EHA should be considered. In this section, the performance degradation input function was designed according to the transfer functions of HA and EHA.

2.2.1. Transfer function of HA and EHA

In the early research,[25] the force fighting problem of DRAS has been studied, similarly with the research work, the variable vector of DRAS was defined as

$$\begin{aligned}\boldsymbol{x}_{\mathrm{DRAS}} &= [x_{11},\ x_{12},\ x_{13},\ x_{14},\ x_{21},\ x_{22},\ x_{23},\ x_{24}]^{\mathrm{T}} \\ &= [x_{\mathrm{h}}, v_{\mathrm{h}}, P_{\mathrm{h}}, x_{\mathrm{v}}, x_{\mathrm{e}}, v_{\mathrm{e}}, P_{\mathrm{e}}, \omega_{\mathrm{e}}]^{\mathrm{T}}\end{aligned} \tag{12}$$

where x_{h} and x_{e} are cylinder piston displacement of HA and EHA respectively; v_{h} and v_{e} are cylinder piston velocity of HA and EHA respectively; P_{h} and P_{e} are loading pressure of HA and EHA respectively; x_{v} is the servo valve spool displacement of HA; and ω_{e} is the motor speed of EHA.

Based on the research work,[25] the state space model of HA can be obtained as

$$\begin{cases}\dot{x}_{11} = x_{12} \\ \dot{x}_{12} = -\frac{B_{\mathrm{h}}+B_{\mathrm{e}}+B_{\mathrm{d}}}{m_{\mathrm{h}}+m_{\mathrm{e}}+m_{\mathrm{d}}}x_{12} + \frac{A_{\mathrm{h}}}{m_{\mathrm{h}}+m_{\mathrm{e}}+m_{\mathrm{d}}}x_{13} \\ \dot{x}_{13} = -\frac{4E_{\mathrm{h}}A_{\mathrm{h}}}{V_{\mathrm{h}}}x_{12} - \frac{4E_{\mathrm{h}}K_{\mathrm{cl}}}{V_{\mathrm{h}}}x_{13} + \frac{4E_{\mathrm{h}}K_{\mathrm{q}}}{V_{\mathrm{h}}}x_{14} \\ \dot{x}_{14} = -\frac{1}{\tau_{\mathrm{v}}}x_{14} + \frac{K_{\mathrm{v}}}{\tau_{\mathrm{v}}}u_1\end{cases} \tag{13}$$

where B_{h}, B_{e} and B_{d} are equivalent damping parameter of hydraulic cylinder piston of HA and EHA, and the control surface respectively; m_{h}, m_{e} and m_{d} are equivalent mass of hydraulic cylinder piston of HA and EHA, and the control surface respectively; A_{h} is the area of HA hydraulic cylinder piston; E_{h} is the volumetric modulus of elasticity of HA; V_{h} is the total volume of the HA hydraulic cylinder; K_{cl} is the sum of flow pressure and leakage coefficient of the HA hydraulic cylinder; K_{q} is the flow change coefficient; K_{v} is the proportionality coefficient of electro-hydraulic servo valve; τ_{v} is the servo valve time constant.

Using Laplace transformation, the transfer function of HA based on its state space model can be obtained as

$$G_{\mathrm{h}}(s) = \frac{X_{\mathrm{h}}(s)}{u_1(s)} = \frac{K_{\mathrm{v}}K_{\mathrm{q}}}{a_{\mathrm{h}}s^4 + b_{\mathrm{h}}s^3 + c_{\mathrm{h}}s^2 + d_{\mathrm{h}}s} \tag{14}$$

where

$$\begin{cases}a_{\mathrm{h}} = \frac{(m_{\mathrm{h}}+m_{\mathrm{e}}+m_{\mathrm{d}})V_{\mathrm{h}}\tau_{\mathrm{v}}}{4E_{\mathrm{h}}A_{\mathrm{h}}} \\ b_{\mathrm{h}} = [V_{\mathrm{h}}\tau_{\mathrm{v}}(B_{\mathrm{h}}+B_{\mathrm{e}}+B_{\mathrm{d}}) + (4E_{\mathrm{h}}\tau_{\mathrm{v}}K_{\mathrm{cl}}+V_{\mathrm{h}}) \\ \qquad \cdot(m_{\mathrm{h}}+m_{\mathrm{e}}+m_{\mathrm{d}})]/4E_{\mathrm{h}}A_{\mathrm{h}} \\ c_{\mathrm{h}} = [(4E_{\mathrm{h}}\tau_{\mathrm{v}}K_{\mathrm{cl}}+V_{\mathrm{h}})(B_{\mathrm{h}}+B_{\mathrm{e}}+B_{\mathrm{d}}) + 4E_{\mathrm{h}}K_{\mathrm{cl}} \\ \qquad \cdot(m_{\mathrm{h}}+m_{\mathrm{e}}+m_{\mathrm{d}})]/4E_{\mathrm{h}}A_{\mathrm{h}} + \tau_{\mathrm{v}}A_{\mathrm{h}} \\ d_{\mathrm{h}} = \frac{(B_{\mathrm{h}}+B_{\mathrm{e}}+B_{\mathrm{d}})k_{\mathrm{cl}}+A_{\mathrm{h}}^2}{A_{\mathrm{h}}}\end{cases}$$

The nomenclature for all the parameters in the equations above is the same as in the research work.[25] Then the dominant pole $s_{\mathrm{H}} = a_{\mathrm{H}}$ which determines the response performance of HA can be obtained.

Still based on the research work,[25] the state space model of EHA can be obtained as

$$\begin{cases}\dot{x}_{21} = x_{22} \\ \dot{x}_{22} = -\frac{B_{\mathrm{h}}+B_{\mathrm{e}}+B_{\mathrm{d}}}{m_{\mathrm{h}}+m_{\mathrm{e}}+m_{\mathrm{d}}}x_{22} + \frac{A_{\mathrm{e}}}{m_{\mathrm{h}}+m_{\mathrm{e}}+m_{\mathrm{d}}}x_{23} \\ \dot{x}_{23} = -\frac{4E_{\mathrm{e}}A_{\mathrm{e}}}{V_{\mathrm{e}}}x_{22} - \frac{4E_{\mathrm{e}}C_{\mathrm{el}}}{V_{\mathrm{e}}}x_{23} + \frac{4E_{\mathrm{e}}V_{\mathrm{P}}}{V_{\mathrm{e}}}x_{24} \\ \dot{x}_{24} = -\frac{V_{\mathrm{P}}}{J_{\mathrm{m}}}x_{23} - \frac{B_{\mathrm{me}}}{J_{\mathrm{m}}}x_{24} + \frac{K_{\mathrm{m}}}{J_{\mathrm{m}}R_{\mathrm{e}}}u_2\end{cases} \tag{15}$$

where A_{e} is the area of EHA hydraulic cylinder piston; E_{e} is the volumetric modulus of elasticity of EHA; V_{e} is the total volume of EHA hydraulic cylinder; C_{el} is the total leakage coefficient of EHA hydraulic cylinder; V_{P} is the pump output of EHA; J_{m} is the total moment of inertia of motor and pump; B_{me} is the simplified equivalent damping coefficient of the motor; K_{m} is the electromagnetic torque constant of the motor; R_{e} is the is the armature resistance of the motor.

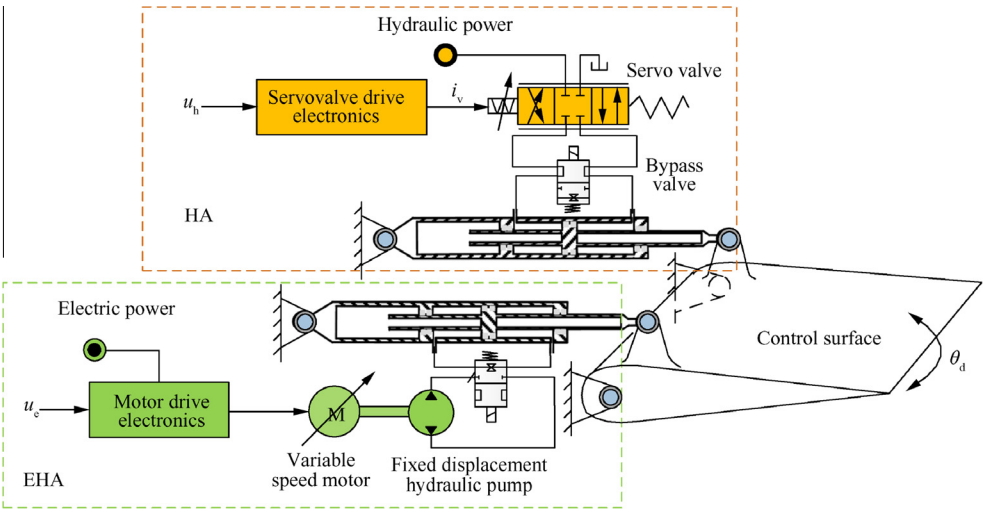

Fig. 5 Dissimilar redundant actuation system composed of HA and EHA.

Using Laplace transformation, the transfer function of EHA based on its state space model can be obtained as

$$G_e(s) = \frac{X_e(s)}{u_2(s)} = \frac{K_m/R_e}{a_e s^4 + b_e s^3 + c_e s^2 + d_e s} \tag{16}$$

where

$$\begin{cases} a_e = \frac{J_m V_e (m_h + m_e + m_d)}{4E_e V_P A_e} \\ b_e = J_m V_e (B_h + B_e + B_d)/4E_e V_P A_e + [(4E_e J_m C_{el} \\ \quad + B_{me} V_e)(m_h + m_e + m_d)]/4E_e V_P A_e \\ c_e = (4E_e J_m C_{el} + B_{me} V_e)(B_h + B_e + B_d)/4E_e V_P A_e \\ \quad + (V_P^2 + B_{me} C_{el})(m_h + m_e + m_d)/V_P A_e \\ \quad + J_m A_e / V_P \\ d_e = \frac{(B_{me} C_{el} + V_P^2)(B_h + B_e + B_d)}{V_P A_e} + \frac{B_{me} A_e}{V_P} \end{cases}$$

The nomenclature for all the parameters in the equations above is also the same as in the research work.[25] Then the dominant pole $s_E = a_E$ which determines the response performance of EHA can be obtained.

2.2.2. Performance degradation input function

In order to compare the response performance of HA and EHA, a signal with the same step for HA and EHA was chosen to be used in simulation. As shown in Fig. 6, EHA responds more slowly than HA.

From the transfer functions of HA and EHA, two dominant poles $s_H = a_H$ and $s_E = a_E$ which determine the response time of HA and EHA respectively can be obtained. Then the degradation performance parameter can be chosen as $\Delta a = |a_H - a_E|$, and then the performance degradation input function can be obtained as

$$\boldsymbol{u}_E = e^{-\Delta a t} \boldsymbol{u}_H \tag{17}$$

In this performance degradation input function, $\boldsymbol{u}_H$ is the input of HA before the aircraft suffers from vertical tail loss, since the dynamics of actuator on control surface is much faster than the system dynamics, which means the control surface deflection bounded in the limit of amplitude can be considered equal to the command generalized by the controller without delay. However, when the aircraft suffers from vertical tail loss, only EHA provides effective measure for the aircraft to actuate the main control surfaces and the response performance degradation $e^{-\Delta a t}$ should be considered.

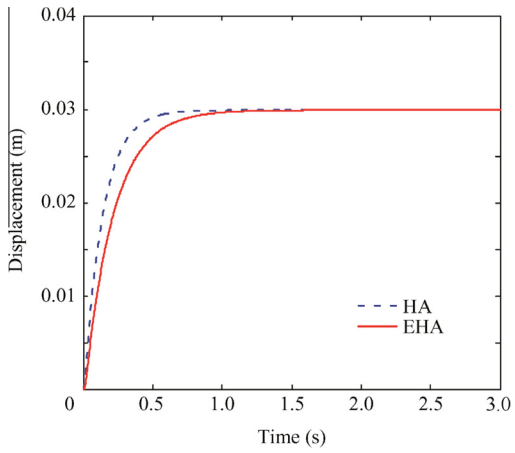

Fig. 6 Response performance comparison of HA and EHA.

2.3. Accurate model of vertical tail damaged aircraft

When the aircraft suffers from vertical tail damage, the corresponding parameters and the input channel all change. Based on the analytical work in the above two sections, the final accurate damaged model can be obtained as

$$\begin{cases} \dot{\boldsymbol{x}} = \boldsymbol{A}(\mu)\boldsymbol{x} + \boldsymbol{B}(\mu)\boldsymbol{u}_E + \boldsymbol{d} \\ \boldsymbol{y} = \boldsymbol{C}\boldsymbol{x} \end{cases} \tag{18}$$

where the state variable vector is still $\boldsymbol{x} = [\beta, \quad p, \quad r, \quad \phi]^T$; $\boldsymbol{d}$ is the external disturbance, and the system matrices are changed into

$$\boldsymbol{A}(\mu) = \begin{bmatrix} \frac{Y_\beta(\mu)}{m} & \frac{Y_p(\mu)}{m} & \frac{Y_r(\mu)}{m} - u_0 & g_0 \cos\theta_0 \\ \frac{L_\beta(\mu)}{I_x} + I'_{zx} N_\beta(\mu) & \frac{L_p(\mu)}{I_x} + I'_{zx} N_p(\mu) & \frac{L_r(\mu)}{I_x} + I'_{zx} N_r(\mu) & 0 \\ \frac{N_\beta(\mu)}{I_z} + I'_{zx} L_\beta(\mu) & \frac{N_p(\mu)}{I_z} + I'_{zx} L_p(\mu) & \frac{N_r(\mu)}{I_z} + I'_{zx} L_r(\mu) & 0 \\ 0 & 1 & \tan\theta_0 & 0 \end{bmatrix},$$

$$\boldsymbol{B}(\mu) = \begin{bmatrix} \frac{Y_{\delta_a}}{m} & \frac{C_{y_\beta}(\mu)}{|C_{y_\beta}(0)|}\left(\frac{Y_{\delta_r}}{m}\right) \\ \frac{L_{\delta_a}}{I_x} + I'_{zx} N_{\delta_a} & \frac{C_{y_\beta}(\mu)}{|C_{y_\beta}(0)|}\left(\frac{L_{\delta_r}}{I_x} + I'_{zx} N_{\delta_r}\right) \\ \frac{N_{\delta_a}}{I_z} + I'_{zx} L_{\delta_a} & \frac{C_{y_\beta}(\mu)}{|C_{y_\beta}(0)|}\left(\frac{N_{\delta_a}}{I_z} + I'_{zx} L_{\delta_r}\right) \\ 0 & 0 \end{bmatrix}$$

where the elements of matrix $\boldsymbol{A}(\mu)$ are calculated using the nonlinear damaged aircraft modeling method which is proposed in Section 2.1. The elements of the second column of matrix $\boldsymbol{B}(\mu)$ change with the damage degree of the rudder, since the shape of the rudder is also regular trapezium which is proportional to the vertical tail, the damage rule is the same as the vertical tail. Therefore, a new damage coefficient $\frac{C_{y_\beta}(\mu)}{|C_{y_\beta}(0)|}$, which is also based on the fundamental equation $C_{y_\beta}(\mu)$, was constructed to obtain the damage matrix $\boldsymbol{B}(\mu)$. The input channel was replaced by the performance degradation input function as shown in Eq. (19).

$$\boldsymbol{u}_E = e^{-\Delta a t} \boldsymbol{u}_H = e^{-\Delta a t} [\delta_a, \quad \delta_r]^T \tag{19}$$

3. Fault-tolerant control strategy

The structure of the FTC strategy is shown in Fig. 7. Under normal condition, the fault detection and isolation (FDI) mechanism would obtain healthy result of the aircraft, and then the baseline control parameters would be solved by the LQR regulator. In this situation, HA systems actuate to maintain desirable flight attitude. Since this paper focuses on the development of AFTC strategy and there are many mature techniques to obtain the fault information, when the vertical tail of the aircraft suffers from partial loss, the damage degree can be assumed to be determined precisely by the FDI mechanism. The corresponding reconfigurable control law would be solved by the LQR regulator. Based on the information from FDI mechanism, the switch mechanism would change the baseline control law into reconfigurable one and launch EHA system for the fault-tolerance of the damaged aircraft. The design steps of the FTC strategy are shown in this section.

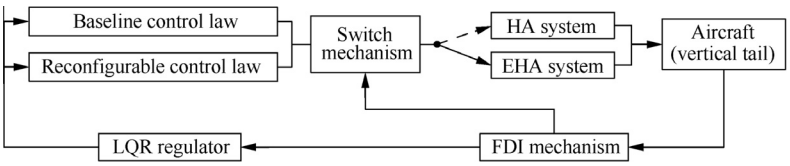

Fig. 7 Structure of FTC strategy.

3.1. Baseline controller design

When all the control surfaces are in good condition, for the plant, a baseline controller was designed according to the following principles: The baseline controller should guarantee the stability of the whole closed loop system; the roll angle can track the given command $r_\phi(t)$, the tracking error $e(t) = r_\phi(t) - \phi(t) \to 0$; meanwhile, the sideslip angle $\beta(t) \to 0°$.

In order to satisfy the design principles, a closed loop feedback control law was designed in good condition as

$$\boldsymbol{u}_{\mathrm{H}} = \boldsymbol{K}_x \boldsymbol{x} + K_\phi \int (r_\phi - \phi)\mathrm{d}t + K_\beta \int (0 - \beta)\,\mathrm{d}t \tag{20}$$

The specific controller structure is shown in Fig. 8.

If the control command was chosen as $\boldsymbol{r} = [r_\phi, \quad r_\beta]^{\mathrm{T}}$ and the plant output was chosen as $\boldsymbol{y} = [\phi, \quad \beta]^{\mathrm{T}}$, then their error $\boldsymbol{e} = \boldsymbol{r} - \boldsymbol{y}$ can be obtained. In order to eliminate the error, a control variable $\boldsymbol{x}_{\mathrm{c}} \in \mathbf{R}^{2\times 1}$ was introduced, and the control variable system should be $\dot{\boldsymbol{x}}_{\mathrm{c}} = \boldsymbol{A}_{\mathrm{c}}\boldsymbol{x}_{\mathrm{c}} + \boldsymbol{B}_{\mathrm{c}}(\boldsymbol{r} - \boldsymbol{y})$. Since the plant output is the controlled object variable vector and the plant follows the control command vector, then the matrices of the control variable system can be chosen as $\boldsymbol{A}_{\mathrm{c}} = \boldsymbol{0}$ and $\boldsymbol{B}_{\mathrm{c}} = \boldsymbol{I}$. Finally an augmented system composed of the plant and the control variable system can be obtained as

$$\begin{cases} \begin{bmatrix} \dot{\boldsymbol{x}} \\ \dot{\boldsymbol{x}}_{\mathrm{c}} \end{bmatrix} = \begin{bmatrix} \boldsymbol{A} & \boldsymbol{0} \\ -\boldsymbol{C} & \boldsymbol{0} \end{bmatrix} \begin{bmatrix} \boldsymbol{x} \\ \boldsymbol{x}_{\mathrm{c}} \end{bmatrix} + \begin{bmatrix} \boldsymbol{B} \\ \boldsymbol{0} \end{bmatrix} \boldsymbol{u}_{\mathrm{H}} + \begin{bmatrix} \boldsymbol{0} \\ \boldsymbol{r} \end{bmatrix} + \begin{bmatrix} \boldsymbol{d} \\ \boldsymbol{0} \end{bmatrix} \\ \boldsymbol{y} = \boldsymbol{\theta} = [\boldsymbol{C} \quad \boldsymbol{0}] \begin{bmatrix} \boldsymbol{x} \\ \boldsymbol{x}_{\mathrm{c}} \end{bmatrix} \end{cases} \tag{21}$$

For this augmented system, the system matrix is $\boldsymbol{A}_{\mathrm{aug}} = \begin{bmatrix} \boldsymbol{A} & \boldsymbol{0} \\ -\boldsymbol{C} & \boldsymbol{0} \end{bmatrix}_{6\times 6}$ and the control matrix is $\boldsymbol{B}_{\mathrm{aug}} = \begin{bmatrix} \boldsymbol{B} \\ \boldsymbol{0} \end{bmatrix}_{6\times 2}$. Then the controllability matrix $\boldsymbol{C}_{\mathrm{con}} = [\boldsymbol{B}_{\mathrm{aug}}, \quad \boldsymbol{A}_{\mathrm{aug}}\boldsymbol{B}_{\mathrm{aug}}, \boldsymbol{A}_{\mathrm{aug}}^2\boldsymbol{B}_{\mathrm{aug}}, \boldsymbol{A}_{\mathrm{aug}}^3\boldsymbol{B}_{\mathrm{aug}}, \boldsymbol{A}_{\mathrm{aug}}^4\boldsymbol{B}_{\mathrm{aug}}, \boldsymbol{A}_{\mathrm{aug}}^5\boldsymbol{B}_{\mathrm{aug}}]$ can be obtained. Using the matrices data in Li and Liu's research work,[10] $\boldsymbol{C}_{\mathrm{con}}$ can be checked as row full rank. Therefore the controllability of the augmented system can be guaranteed. And then, a control law can be designed for poles' assignment so that the closed loop system poles can guarantee the system stability. After poles assignment by the control law form $\boldsymbol{u}_{\mathrm{H}} = \boldsymbol{K}_x\boldsymbol{x} + \boldsymbol{K}_{\mathrm{c}}\boldsymbol{x}_{\mathrm{c}}$, the closed loop poles of system can have negative real part. The control law form as in Eq. (20) can be obtained by defining $\boldsymbol{K}_{\mathrm{c}} = [K_\phi, \quad K_\beta]$. With the control law Eq. (20), which is essentially a PI controller, the system can track the command with no steady-error. By solving reasonable feedback gain $\boldsymbol{K}_x$ and $\boldsymbol{K}_{\mathrm{c}}$, the system can have a better dynamic performance. LQR technique was applied in this paper to calculate the feedback gain $\boldsymbol{K}_x$ and $\boldsymbol{K}_{\mathrm{c}}$. The control law can be conveniently obtained by selecting the state weighting matrix $\boldsymbol{Q}$ and input weighting matrix $\boldsymbol{R}$, whose objective is to minimize the total control cost, which can be formally stated as

$$J = \frac{1}{2}\int_0^\infty (\boldsymbol{x}_{\mathrm{aug}}^{\mathrm{T}}\boldsymbol{Q}\boldsymbol{x}_{\mathrm{aug}} + \boldsymbol{u}_{\mathrm{H}}^{\mathrm{T}}\boldsymbol{R}\boldsymbol{u}_{\mathrm{H}})\mathrm{d}t \tag{22}$$

where $\boldsymbol{x}_{\mathrm{aug}} = [\boldsymbol{x}, \quad \boldsymbol{x}_{\mathrm{c}}]^{\mathrm{T}}$ and $\boldsymbol{u}_{\mathrm{H}}$ is the input vector with HA; the optimal solution to minimize the total control cost can be obtained by solving the following Riccati Equation:

$$\boldsymbol{P}\boldsymbol{A}_{\mathrm{aug}} + \boldsymbol{A}_{\mathrm{aug}}^{\mathrm{T}}\boldsymbol{P} - \boldsymbol{P}\boldsymbol{B}_{\mathrm{aug}}\boldsymbol{R}^{-1}\boldsymbol{B}_{\mathrm{aug}}^{\mathrm{T}}\boldsymbol{P} + \boldsymbol{Q} = \boldsymbol{0} \tag{23}$$

where the matrix $\boldsymbol{P}$ is positive and definite. Then the feedback gain $\boldsymbol{K}_x$ and $\boldsymbol{K}_{\mathrm{c}}$ can be solved as

$$[\boldsymbol{K}_x, \quad \boldsymbol{K}_{\mathrm{c}}] = -\boldsymbol{R}^{-1}\boldsymbol{B}_{\mathrm{aug}}^{\mathrm{T}}\boldsymbol{P} \tag{24}$$

3.2. Reconfigurable controller design and adaptive parameter adjustment

When the aircraft suffers from vertical tail damage, the input channel of HA system would lose its ability to actuate; meanwhile, several stability derivatives change. In this situation, the baseline control law may not be robust enough to tolerate the fault to maintain a graceful flight performance, and may even

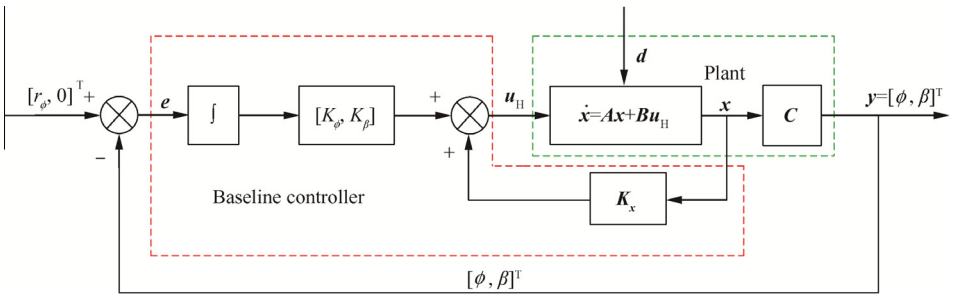

Fig. 8 Lateral-directional baseline control law.

threaten the flight safety. Therefore, another reconfigurable controller should be designed to stabilize the damaged aircraft model and realize required function reconfiguration. Since the severe loss of vertical tail occurs, the rudder would not continue to provide yaw function and the aileron's roll function can be used to provide the centripetal force to realize the yaw function finally. First, the reconfigurable control gain is resolved using LQR technique and then MRAC method is used to adjust the solved control gain, which can guarantee that the reconfigurable control law is more effective. MRAC mechanism designed in this paper is shown in Fig. 9.

The reference model can be expressed in the following form:

$$\begin{cases} \dot{\boldsymbol{x}}_{\mathrm{m}} = \boldsymbol{A}_{\mathrm{m}}\boldsymbol{x}_{\mathrm{m}} + \boldsymbol{B}_{\mathrm{m}}\boldsymbol{u}_{\mathrm{m}} \\ \boldsymbol{y}_{\mathrm{m}} = \boldsymbol{C}_{\mathrm{m}}\boldsymbol{x}_{\mathrm{m}} \end{cases} \tag{25}$$

This is a closed loop system controlled by the baseline controller. As an reference model, the system matrices can be deduced as $\boldsymbol{A}_{\mathrm{m}} = \begin{bmatrix} \boldsymbol{A}+\boldsymbol{B}\boldsymbol{K}_x & \boldsymbol{B}\boldsymbol{K}_{\mathrm{c}} \\ -\boldsymbol{C} & \boldsymbol{0} \end{bmatrix}_{6\times6}$, $\boldsymbol{B}_{\mathrm{m}} = \begin{bmatrix} \boldsymbol{0}_{4\times2} \\ \boldsymbol{I} \end{bmatrix}_{6\times2}$, $\boldsymbol{C}_{\mathrm{m}} = \begin{bmatrix} 0 & 0 & 0 & 1 & 0 & 0 \\ 1 & 0 & 0 & 0 & 0 & 0 \end{bmatrix}_{2\times6}$. $\boldsymbol{x}_{\mathrm{m}} = [\boldsymbol{x}, \quad \boldsymbol{x}_{\mathrm{c}}]^{\mathrm{T}}_{6\times1}$ is the state variable vector, $\boldsymbol{u}_{\mathrm{m}} = \boldsymbol{r}_{\mathrm{update}} = [r_\phi, \quad r_\beta]^{\mathrm{T}}$ is the latest command vector and $\boldsymbol{y} = [\phi, \quad \beta]^{\mathrm{T}}$ is the system output. When the aircraft suffers from vertical tail damage, a control variable $\dot{\boldsymbol{x}}_{\mathrm{c}} = \boldsymbol{r} - \boldsymbol{y}$ was introduced as done to the reference model, and then the plant was obtained as

$$\begin{cases} \dot{\boldsymbol{x}}_{\mathrm{p}} = \boldsymbol{A}_{\mathrm{p}}\boldsymbol{x}_{\mathrm{p}} + \boldsymbol{B}_{\mathrm{p}}\boldsymbol{u}_{\mathrm{p}} + \boldsymbol{d}_{\mathrm{l}} + \boldsymbol{B}_{\mathrm{r}}\boldsymbol{r}_{\mathrm{update}} \\ \boldsymbol{y}_{\mathrm{p}} = \boldsymbol{C}_{\mathrm{p}}\boldsymbol{x}_{\mathrm{p}} \end{cases} \tag{26}$$

where $\boldsymbol{A}_{\mathrm{p}} = \begin{bmatrix} \boldsymbol{A}(\mu) & \boldsymbol{0} \\ -\boldsymbol{C} & \boldsymbol{0} \end{bmatrix}_{6\times6}$, $\boldsymbol{B}_{\mathrm{p}} = \begin{bmatrix} \boldsymbol{B}(\mu) \\ \boldsymbol{0} \end{bmatrix}_{6\times2}$, $\boldsymbol{B}_{\mathrm{r}} = \begin{bmatrix} \boldsymbol{0}_{4\times2} \\ \boldsymbol{I} \end{bmatrix}_{6\times2}$, $\boldsymbol{C}_{\mathrm{p}} = \begin{bmatrix} 0 & 0 & 0 & 1 & 0 & 0 \\ 1 & 0 & 0 & 0 & 0 & 0 \end{bmatrix}_{2\times6}$, $\boldsymbol{d}_{\mathrm{l}} = \begin{bmatrix} \boldsymbol{d}_{4\times1} \\ \boldsymbol{0}_{2\times1} \end{bmatrix}$.

Since the plant and its reference model have the same dimension, model following method can be applied to designing the fault tolerant control strategy.

The error between the state of reference model Eq. (25) and plant Eq. (26) can be defined as $\boldsymbol{e}_{\mathrm{ref}} = \boldsymbol{x}_{\mathrm{m}} - \boldsymbol{x}_{\mathrm{p}}$, and the control input form was chosen as

$$\boldsymbol{u}_{\mathrm{p}} = \boldsymbol{K}_{\mathrm{e}}\boldsymbol{e}_{\mathrm{ref}} + \boldsymbol{K}_{\mathrm{m}}\boldsymbol{x}_{\mathrm{m}} + \Delta\boldsymbol{U}_{\mathrm{d}} \tag{27}$$

where $\boldsymbol{K}_{\mathrm{e}}$ and $\boldsymbol{K}_{\mathrm{m}}$ are control gain matrices which need to be solved and $\Delta\boldsymbol{U}_{\mathrm{d}}$ is the input compensation which mainly deals with the outside interference $\boldsymbol{d}_{\mathrm{l}}$ in Eq. (26).

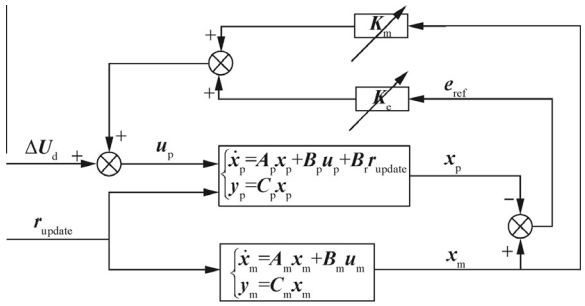

Fig. 9 Mechanism of model reference adaptive control method.

Then the differential of state error can be written as

$$\begin{aligned} \dot{\boldsymbol{e}}_{\mathrm{ref}} &= \dot{\boldsymbol{x}}_{\mathrm{m}} - \dot{\boldsymbol{x}}_{\mathrm{p}} = \boldsymbol{A}_{\mathrm{p}}\boldsymbol{e}_{\mathrm{ref}} + (\boldsymbol{A}_{\mathrm{m}} - \boldsymbol{A}_{\mathrm{p}})\boldsymbol{x}_{\mathrm{m}} + \boldsymbol{B}_{\mathrm{m}}\boldsymbol{u}_{\mathrm{m}} - \boldsymbol{B}_{\mathrm{p}}\boldsymbol{u}_{\mathrm{p}} \\ &\quad - \boldsymbol{B}_{\mathrm{r}}\boldsymbol{r}_{\mathrm{update}} - \boldsymbol{d}_{\mathrm{l}} = (\boldsymbol{A}_{\mathrm{p}} - \boldsymbol{B}_{\mathrm{p}}\boldsymbol{K}_{\mathrm{e}})\boldsymbol{e}_{\mathrm{ref}} + (\boldsymbol{A}_{\mathrm{m}} - \boldsymbol{A}_{\mathrm{p}} - \boldsymbol{B}_{\mathrm{p}}\boldsymbol{K}_{\mathrm{m}})\boldsymbol{x}_{\mathrm{m}} \\ &\quad + (\boldsymbol{B}_{\mathrm{m}}\boldsymbol{u}_{\mathrm{m}} - \boldsymbol{B}_{\mathrm{r}}\boldsymbol{r}_{\mathrm{update}}) - (\boldsymbol{B}_{\mathrm{p}}\Delta\boldsymbol{U}_{\mathrm{d}} + \boldsymbol{d}_{\mathrm{l}}) = (\boldsymbol{A}_{\mathrm{p}} - \boldsymbol{B}_{\mathrm{p}}\boldsymbol{K}_{\mathrm{e}})\boldsymbol{e}_{\mathrm{ref}} \\ &\quad + (\boldsymbol{A}_{\mathrm{m}} - \boldsymbol{A}_{\mathrm{p}} - \boldsymbol{B}_{\mathrm{p}}\boldsymbol{K}_{\mathrm{m}})\boldsymbol{x}_{\mathrm{m}} - (\boldsymbol{B}_{\mathrm{p}}\Delta\boldsymbol{U}_{\mathrm{d}} + \boldsymbol{d}_{\mathrm{l}}) \end{aligned} \tag{28}$$

By choosing appropriate gain matrix $\boldsymbol{K}_{\mathrm{m}} \in \mathbf{R}^{2\times6}$ and $\Delta\boldsymbol{U}_{\mathrm{d}}$ to satisfy the relationship described by Eq. (27),

$$\begin{cases} \boldsymbol{A}_{\mathrm{m}} - \boldsymbol{A}_{\mathrm{p}} - \boldsymbol{B}_{\mathrm{p}}\boldsymbol{K}_{\mathrm{m}} = \boldsymbol{0} \\ \boldsymbol{B}_{\mathrm{p}}\Delta\boldsymbol{U}_{\mathrm{d}} + \boldsymbol{d}_{\mathrm{l}} = \boldsymbol{0} \end{cases} \tag{29}$$

it leads to

$$\dot{\boldsymbol{e}}_{\mathrm{ref}} = (\boldsymbol{A}_{\mathrm{p}} - \boldsymbol{B}_{\mathrm{p}}\boldsymbol{K}_{\mathrm{e}})\boldsymbol{e}_{\mathrm{ref}} \tag{30}$$

By checking the controllability of $(\boldsymbol{A}_{\mathrm{p}}, \boldsymbol{B}_{\mathrm{p}})$ and the poles of matrix $\boldsymbol{A}_{\mathrm{p}} - \boldsymbol{B}_{\mathrm{p}}\boldsymbol{K}_{\mathrm{e}}$ have negative real part, the error $\boldsymbol{e}_{\mathrm{ref}} = \boldsymbol{x}_{\mathrm{m}} - \boldsymbol{x}_{\mathrm{p}}$ can be controlled to be zero.

The original feedback control gain matrices $\boldsymbol{K}_{\mathrm{e}}$ and $\boldsymbol{K}_{\mathrm{m}}$ were calculated through the plant matrices $\boldsymbol{A}(\mu)$ and $\boldsymbol{B}(\mu)$ in theory. $\Delta\boldsymbol{U}_{\mathrm{d}}$ was chosen following a certain adaptive adjustment law. Due to the parameter errors between the plant and the actual system, their closed loop dynamic performance may behave very differently. Adaptive parameter adjustment was used to realize the same dynamic performance, which leads the control law to be more efficient.

The adaptive parameter adjustment law is designed in the following process:

$$\begin{aligned} \dot{\boldsymbol{e}}_{\mathrm{ref}} &= \dot{\boldsymbol{x}}_{\mathrm{m}} - \dot{\boldsymbol{x}}_{\mathrm{p}} \\ &= (\boldsymbol{A}_{\mathrm{p}} - \boldsymbol{B}_{\mathrm{p}}\boldsymbol{K}_{\mathrm{e}})\boldsymbol{e}_{\mathrm{ref}} + (\boldsymbol{A}_{\mathrm{m}} - \boldsymbol{A}_{\mathrm{p}} - \boldsymbol{B}_{\mathrm{p}}\boldsymbol{K}_{\mathrm{m}})\boldsymbol{x}_{\mathrm{m}} \\ &\quad - (\boldsymbol{B}_{\mathrm{p}}\Delta\boldsymbol{U}_{\mathrm{d}} + \boldsymbol{d}_{\mathrm{l}}) \\ &= \overline{\boldsymbol{A}_{\mathrm{p}}}\boldsymbol{e}_{\mathrm{ref}} + \boldsymbol{B}_{\mathrm{p}}(\boldsymbol{K}_{\mathrm{e}}(t) - \boldsymbol{K}_{\mathrm{e}}(0))\boldsymbol{e}_{\mathrm{ref}} \\ &\quad + \boldsymbol{B}_{\mathrm{p}}(\boldsymbol{K}_{\mathrm{m}}(t) - \boldsymbol{K}_{\mathrm{m}}(0))\boldsymbol{x}_{\mathrm{m}} - \boldsymbol{B}_{\mathrm{p}}(\Delta\boldsymbol{U}_{\mathrm{d}}(\mathbf{t}) - \Delta\boldsymbol{U}_{\mathrm{d}}(0)) \\ &= \overline{\boldsymbol{A}_{\mathrm{p}}}\boldsymbol{e}_{\mathrm{ref}} + \boldsymbol{B}_{\mathrm{p}}\boldsymbol{\Phi}\boldsymbol{e}_{\mathrm{ref}} + \boldsymbol{B}_{\mathrm{p}}\boldsymbol{\Psi}\boldsymbol{x}_{\mathrm{m}} + \boldsymbol{B}_{\mathrm{p}}\boldsymbol{\zeta} \end{aligned} \tag{31}$$

where $\boldsymbol{\Phi} = \boldsymbol{K}_{\mathrm{e}}(t) - \boldsymbol{K}_{\mathrm{e}}(0)$, $\boldsymbol{\Psi} = \boldsymbol{K}_{\mathrm{m}}(t) - \boldsymbol{K}_{\mathrm{m}}(0)$, $\boldsymbol{\zeta} = \Delta\boldsymbol{U}_{\mathrm{d}}(t) - \Delta\boldsymbol{U}_{\mathrm{d}}(0)$.

By defining Lyapunov function as

$$V = \frac{1}{2}\left[\boldsymbol{e}_{\mathrm{ref}}^{\mathrm{T}}\boldsymbol{P}_{\mathrm{adap}}\boldsymbol{e}_{\mathrm{ref}} + \mathrm{tr}(\boldsymbol{\Phi}^{\mathrm{T}}\boldsymbol{\Gamma}_1^{-1}\boldsymbol{\Phi} + \boldsymbol{\Psi}^{\mathrm{T}}\boldsymbol{\Gamma}_2^{-1}\boldsymbol{\Psi} + \boldsymbol{\zeta}^{\mathrm{T}}\boldsymbol{\Gamma}_3^{-1}\boldsymbol{\zeta})\right] \tag{32}$$

where $\boldsymbol{P}_{\mathrm{adap}} \in \mathbf{R}^{6\times6}$, $\boldsymbol{\Gamma}_1 \in \mathbf{R}^{6\times6}$, $\boldsymbol{\Gamma}_2 \in \mathbf{R}^{6\times6}$ and $\boldsymbol{\Gamma}_3 \in \mathbf{R}^{6\times6}$ are all positive definite symmetric matrices. Based on the Lyapunov function shown in Eq. (32), the adaptive law can be obtained as

$$\begin{cases} \boldsymbol{u}_{\mathrm{p}}(t) = \boldsymbol{K}_{\mathrm{e}}(t)\boldsymbol{e}_{\mathrm{ref}}(t) + \boldsymbol{K}_{\mathrm{m}}(t)\boldsymbol{x}_{\mathrm{m}}(t) + \Delta\boldsymbol{U}_{\mathrm{d}} \\ \boldsymbol{K}_{\mathrm{e}}(t) = \int_0^t (\boldsymbol{e}_{\mathrm{ref}}\boldsymbol{e}_{\mathrm{ref}}^{\mathrm{T}}\boldsymbol{P}_{\mathrm{adap}}\boldsymbol{B}_{\mathrm{p}}\boldsymbol{\Gamma}_1)^{\mathrm{T}}\mathrm{d}\tau + \boldsymbol{K}_{\mathrm{e}}(0) \\ \boldsymbol{K}_{\mathrm{m}}(t) = \int_0^t (\boldsymbol{x}_{\mathrm{m}}\boldsymbol{e}_{\mathrm{ref}}^{\mathrm{T}}\boldsymbol{P}_{\mathrm{adap}}\boldsymbol{B}_{\mathrm{p}}\boldsymbol{\Gamma}_2)^{\mathrm{T}}\mathrm{d}\tau + \boldsymbol{K}_{\mathrm{m}}(0) \\ \Delta\boldsymbol{U}_{\mathrm{d}}(t) = \int_0^t (\boldsymbol{e}_{\mathrm{ref}}^{\mathrm{T}}\boldsymbol{P}_{\mathrm{adap}}\boldsymbol{B}_{\mathrm{p}}\boldsymbol{\Gamma}_3)^{\mathrm{T}}\mathrm{d}\tau + \Delta\boldsymbol{U}_{\mathrm{d}}(0) \end{cases} \tag{33}$$

where $\boldsymbol{K}_{\mathrm{e}}(0)$, $\boldsymbol{K}_{\mathrm{m}}(0)$ and $\Delta\boldsymbol{U}_{\mathrm{d}}(0)$ are the initial values; $\boldsymbol{K}_{\mathrm{e}}(t)$, $\boldsymbol{K}_{\mathrm{m}}(t)$ and $\Delta\boldsymbol{U}_{\mathrm{d}}(t)$ are the current moment value obtained through the designed adaptive law.

4. Simulation study

4.1. Flight conditions and data

To verify the modeling and the effectiveness of the proposed method in this paper, it was used on the Boeing 747 lateral-directional model. The given model is in steady flight of certain flight condition. The data are listed in Table 1.[10]

4.2. Simulation results

4.2.1. Simulation for effectiveness of baseline control law

First, the baseline control law parameters was solved using the proposed fault-tolerant strategy and LQR technique, and then its effectiveness was verified in normal conditions. The specific expressions for system coefficients $\boldsymbol{A}$ and $\boldsymbol{B}$ were given as

$$\begin{cases} \boldsymbol{A} = \begin{bmatrix} -0.1068 & 0 & -673.0000 & 32.1804 \\ -3.5276 & -0.8442 & 0.3088 & 0 \\ 3.6534 & -0.0401 & -0.2479 & 0 \\ 0 & 1 & 0.0349 & 0 \end{bmatrix} \\ \boldsymbol{B} = \begin{bmatrix} 0 & 9.5858 \\ 0.2219 & 0.1030 \\ 0.0155 & -0.6208 \\ 0 & 0 \end{bmatrix} \end{cases} \tag{34}$$

The baseline control law parameter matrix was solved as

$$\boldsymbol{K}_{\text{base}}(0) = \begin{bmatrix} -0.1396 & 12.5755 & 3.0829 & 19.5440 & -9.3071 & -3.6576 \\ 31.3745 & -4.5693 & -60.8569 & -4.4717 & 3.6576 & -9.3071 \end{bmatrix} \tag{35}$$

Fig. 10 shows the system dynamic performance in normal conditions. As shown in Fig. 10(a), a sine wave signal with peak value of $\pm 12^\circ$ was given to the model as the roll command. The roll angel response can track the command well with acceptable time delay, meanwhile, the fluctuation amplitude of the sideslip angel is limited in $\pm 0.1^\circ$ and can be regarded as zero steady state.

Table 1 Flight condition, aircraft parameters and derivatives.

Aircraft property		Lateral-directional	
Altitude (km)	6.096	C_{l_β} (1/rad)	−0.16
Air density (kg/m^3)	0.654	C_{l_p} (1/rad)	−0.34
Speed (m/s)	205.1304	C_{l_r} (1/rad)	0.13
Wing area (m^2)	510.967	$C_{l_{\delta_a}}$ (1/rad)	0.013
Wing span (m)	59.7408	$C_{l_{\delta_r}}$ (1/rad)	0.003
Wing mean chord (m)	8.3210	C_{n_β} (1/rad)	0.16
Weight (kg)	288771.723	C_{n_p} (1/rad)	−0.026
I_{xx}(kg · m^2)	24.6759×10^6	C_{n_r} (1/rad)	−0.28
I_{yy}(kg · m^2)	44.8776×10^6	$C_{n_{\delta_a}}$ (1/rad)	−0.0018
I_{zz}(kg · m^2)	67.3841×10^6	$C_{n_{\delta_r}}$ (1/rad)	−0.100
I_{xz}(kg · m^2)	1.3151×10^6	C_{y_β} (1/rad)	−0.90
Air velocity (m/s)	205.1304	C_{y_p}	0
Thrust (N)	43903.734	C_{y_r}	0
Air density (kg/m^3)	0.654	$C_{y_{\delta_a}}$	0
Pressure ratio	0.4695	$C_{y_{\delta_r}}$	0.12

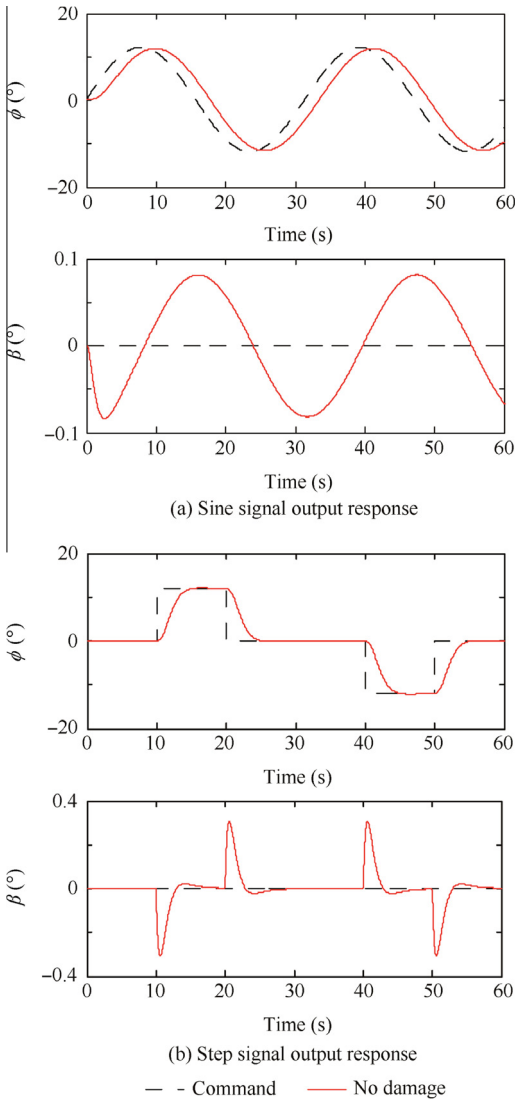

Fig. 10 System dynamic performance in normal condition.

As shown in Fig. 10(b), when given a step signal of 12° during 10–20 s and 40–50 s as the roll command, during the control process, the roll response curve can track the command well and the sideslip angle can steady at zero value finally.

The above simulation results illustrate the effectiveness of the baseline control law design.

4.2.2. Simulation for comparisons between modeling and fault-tolerant control methods

In this section, three methods were chosen to compare with each other to illustrate the control improvement of the nonlinear modeling method and the effectiveness of the proposed AFTC method. Notations for the three methods were made as follows.

Method 1 (M_1): PFTC method (guaranteed cost control with robust pole placement) with linear modeling for the damaged aircraft model in Ref.[10].

Method 2 (M_2): AFTC method (MRAC composed with LQR regulator) with linear modeling for the damaged aircraft model.

Method 3 (M_3): AFTC method (MRAC composed with LQR regulator) with nonlinear accurate modeling for the damaged aircraft proposed in this paper.

The absolute difference $|\Delta C_{y_\beta}|$ reaches the maximum value when the damage degree $\mu = 0.9$, it means the modeling error also reaches the maximum value, therefore, the linear and nonlinear modeling methods were compared at $\mu = 0.9$.

The system coefficient matrices using linear modeling method were obtained as

$$\begin{cases} \boldsymbol{A}_{\text{linear}}(0.9) = \begin{bmatrix} 9.9433 & 1.2081 & -679.3420 & 32.1804 \\ -3.3920 & -0.8041 & 0.1275 & 0 \\ -2.6928 & -0.0988 & -0.0607 & 0 \\ 0 & 1 & 0.0349 & 0 \end{bmatrix} \\ \boldsymbol{B}_{\text{linear}}(0.9) = \begin{bmatrix} 0 & 0.9586 \\ 0.2219 & 0.0103 \\ 0.0155 & -0.0621 \\ 0 & 0 \end{bmatrix} \end{cases} \tag{36}$$

It has been proved that M_1 has obvious effectiveness when the damage degree is not very serious.[10] In this paper the damage degree $\mu = 0.9$ was chosen to verify the control result of the PFTC method compared with the AFTC ones. LMI constraint conditions in Ref.[10] were solved to obtain the control parameter matrix of M_1 as

$$\boldsymbol{K}_{\text{linear}}^{\text{PFTC}}(0.9) = \begin{bmatrix} -16.6368 & 3.6721 & -12.0535 & 0.5426 \\ -10.5161 & -1.2579 & 705.1688 & -33.4036 \end{bmatrix} \tag{37}$$

The initial control parameter matrix of M_2 was solved using LQR regulator as

$$\boldsymbol{K}_{\text{linear}}^{\text{PFTC}}(0.9) = \begin{bmatrix} -5.8781 & 1.7012 & 80.8187 & -2.0381 & -0.3106 & -0.0592 \\ 51.4982 & 3.0704 & -730.0424 & 34.2196 & 0.0592 & -0.3106 \end{bmatrix} \tag{38}$$

The system coefficient matrices using the proposed nonlinear modeling method were obtained as

$$\begin{cases} \boldsymbol{A}_{\text{nonlinear}}(0.9) = \begin{bmatrix} 5.5883 & 0.6846 & -676.5938 & 32.1804 \\ -3.4507 & -0.8215 & 0.2061 & 0 \\ 0.0572 & -0.0734 & -0.0729 & 0 \\ 0 & 1 & 0.0349 & 0 \end{bmatrix} \\ \boldsymbol{B}_{\text{nonlinear}}(0.9) = \begin{bmatrix} 0 & 4.6970 \\ 0.2219 & 0.0505 \\ 0.0155 & -0.3042 \\ 0 & 0 \end{bmatrix} \end{cases} \tag{39}$$

The initial corresponding fault tolerant control parameter matrix of M_3 was solved as

$$\boldsymbol{K}_{\text{nonlinear}}^{\text{AFTC}}(0.9) = \begin{bmatrix} -0.0651 & 0.1449 & 2.6504 & 0.0422 & -0.0345 & -0.3143 \\ 1.6655 & -0.3998 & -65.5610 & -2.7763 & 0.3143 & -0.0345 \end{bmatrix} \tag{40}$$

In this section, a sine wave signal and a step signal were used in simulations and the control results of M_1, M_2 and M_3 were compared with each other. Fig. 11 shows the system dynamics performance comparison between PFTC and AFTC methods. The analysis for the simulation results are as follows.

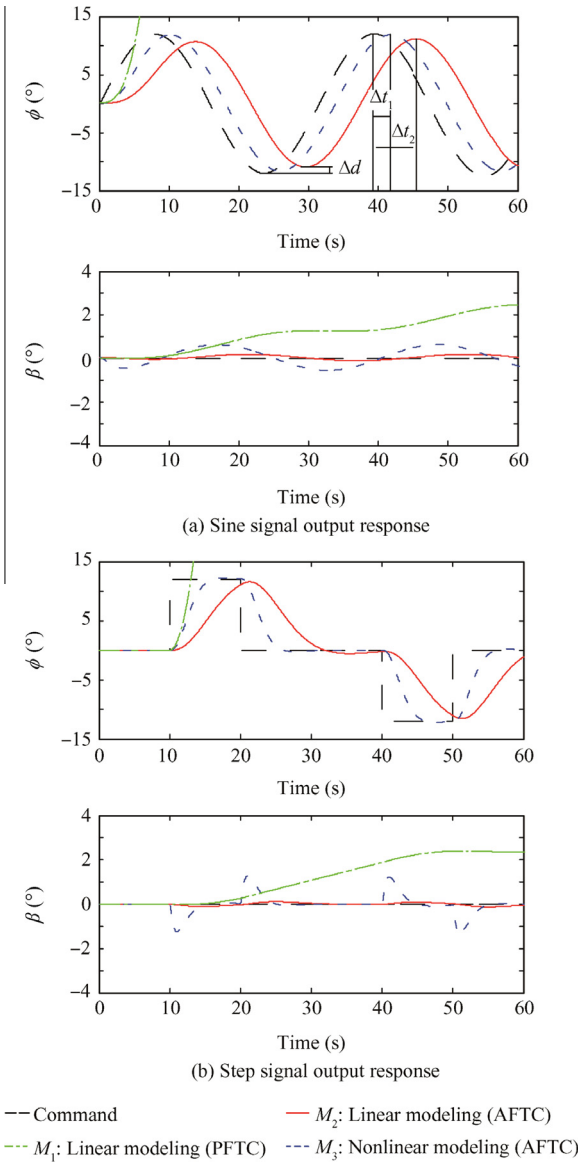

Fig. 11 System dynamics performance using PFTC and AFTC with $\mu = 0.9$.

When giving the damaged model a sine wave signal, the output responses using M_1, M_2 and M_3 are shown in Fig. 11(a). First, the control results of M_1 and M_2 were compared: using M_1 to control the damaged model, the roll angle can hardly track the command signal and diverge to extremely serious degree, meanwhile, the sideslip angle also presents divergent trend. Air crash would happen in this situation. Simulation results illustrate that it is futile to use M_1 to control the damaged model to serious damage degree, and the aircraft would crash due to extreme rolling act. Compared with M_1, when using M_2, though time delay exists, the roll response can track the command with small sideslip angle mostly. It illustrates that when the damage degree is serious to some certain extent, AFTC method is more efficient and can avoid air crash. Second, the control results of M_2 and M_3 were com-

pared: compared with M_2, though the fluctuation amplitude in sideslip response is a little bigger, it is very small and acceptable. Meanwhile, the time delay of tracking performance is obviously shorter since $\Delta t_2 > 2\Delta t_1$; besides, using M_3 can eliminate the wave error Δd. This comparison illustrates that based on the proposed nonlinear accurate modeling model, the control performance for the damaged aircraft model can be improved.

The roll command signal was chosen in the form of steps during 10–20 s and 40–50 s. The output responses using M_1, M_2 and M_3 are all shown in Fig. 11(b). First, the control results of M_1 and M_2 were compared: similarly to the sine wave signal condition, using M_1 to control the damaged model, the roll angle can hardly track the command signal and diverge to extremely serious degree; meanwhile, the sideslip angel also presents divergent trend. Simulation results illustrate that it is futile to use M_1 to control the damaged model when $\mu = 0.9$, the aircraft would crash due to extreme rolling act. Compared with M_1, when using M_2, the sideslip angle can stabilize near zero value and the roll response does not diverge; however, the tracking performance is still very bad. This comparison illustrates that when the damage degree is serious to some certain extent, AFTC method is very necessary. Second, the control results of M_2 and M_3 were compared: compared with M_2, though there exist fluctuations in sideslip response, the fluctuation amplitude and the frequency are very small and acceptable; meanwhile, the tracking performance of the roll angle is obviously better than that using M_2. This comparison illustrates that based on the proposed nonlinear accurate modeling model, the control performance for the damaged aircraft model can be improved.

4.2.3. Simulation for effectiveness of AFTC method in maximum damage condition

In this section, the control effectiveness of the proposed AFTC method in maximum damage condition was verified. The damage degree was chosen as $\mu = 1.0$, which means the aircraft totally lose the whole vertical tail. The damaged model matrices and the control law matrix were calculated as

$$\begin{cases} \boldsymbol{A}(1) = \begin{bmatrix} 11.0600 & 1.3423 & -680.0467 & 32.1804 \\ -3.3769 & -0.7996 & 0.1074 & 0 \\ -3.3979 & -0.1053 & -0.0952 & 0 \\ 0 & 1 & 0.0349 & 0 \end{bmatrix} \\ \boldsymbol{B}(1) = \begin{bmatrix} 0 & 0 \\ 0.2219 & 0 \\ 0.0155 & 0 \\ 0 & 0 \end{bmatrix} \end{cases} \tag{41}$$

$$\boldsymbol{K}_{\text{critical}}(1) = \begin{bmatrix} -625.2264 & -52.5985 & 7.9109 \times 10^3 & -395.5052 & 10.0000 & 0.0134 \\ 0 & 0 & 0 & 0 & 0 & 0 \end{bmatrix} \tag{42}$$

Fig. 12 shows the system dynamic performance under AFTC control law in maximum damage condition. As shown in Fig. 12(a), when the vertical tail damage degree $\mu = 1.0$, using the AFTC method, a sine wave signal was given to the damaged model, the roll angle response can track the command well with acceptable time delay; meanwhile, though the sideslip angle response has sine wave fluctuation, the fluctuation amplitude is limited to be $\pm 0.1^\circ$ and can be regarded as zero steady state.

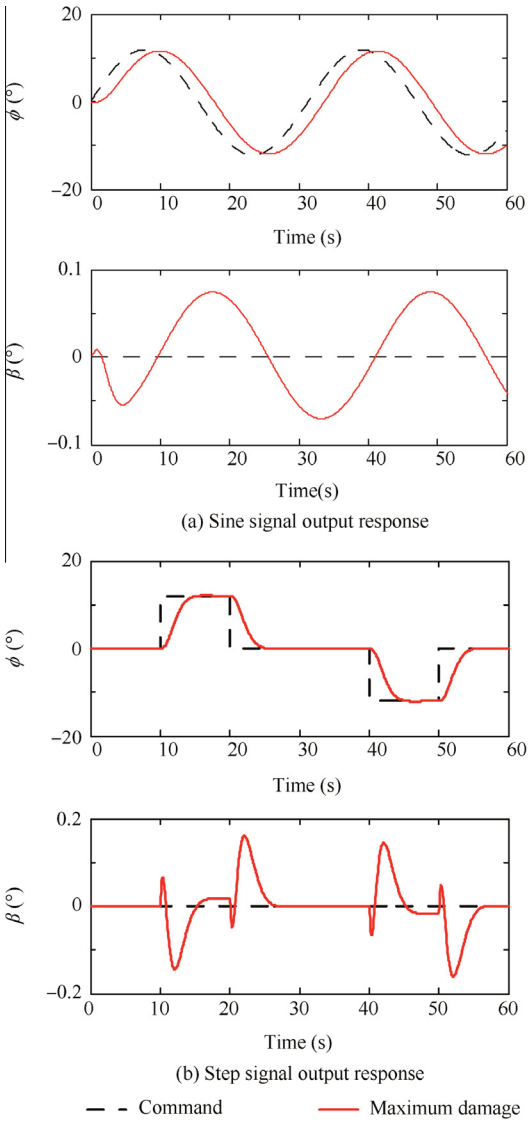

Fig. 12 System dynamic performance under AFTC control law in maximum damage condition.

As shown in Fig. 12(b), when the vertical tail damage degree $\mu = 1.0$, using the AFTC method, a step signal of 12° during 10–20 s and 40–50 s was given to the damaged model as the roll command, the roll angle response can track the command well; meanwhile, though the sideslip angle response has higher fluctuation frequency than before, the fluctuation amplitude is limited to be $\pm 0.2^\circ$ and finally stabilized at zero value.

The simulation results shown in Fig. 12 illustrate that even in the most serious damage degree, the proposed AFTC method can maintain the damaged aircraft controllable and safe.

5. Conclusions

In this paper, the modeling and control of new-type civil aircraft under vertical tail damage condition have been studied and evaluated.

(1) The fault tolerant control capability of aircrafts with DRAS to respond to extraordinary situations is discussed. A damage degree coefficient based on the effective vertical tail area is introduced, and then the nonlinear relationship between the damage degree and its relevant stability and control derivatives are studied. Meanwhile, the performance of EHA is also modeled in the damaged dynamic model. Considering these two factors, an accurate damaged dynamic model is developed.
(2) The fault tolerant control strategy for the damaged aircraft model with vertical tail loss is studied. Based on the accurate modeling, the fault tolerant strategy, using MRAC composed with LQR technique, is developed. In this way, the control law parameters can be determined by LQR method more efficiently and can be adjusted using MRAC to be more precise in fault condition. Simulation results to different damage degrees indicate the effectiveness of the fault tolerant control strategy.
(3) Our further research will focus on the problem of fault degree detection and isolation, and then integrate the FDI technique with the fault tolerant strategy efficiently. Based on this comprehensive technology, our fault tolerant strategies may be more applicable.

Acknowledgements

This work was supported by the National Basic Research Program of China (No 2014CB046402), the National Natural Science Foundation of China (No. 51575019) and 111 Project of China.

References

1. Crider LD. Control of commercial aircraft with vertical tail loss. *Proceedings of AIAA 4th aviation technology, integration, and operation (ATIO) forum*. 2004 Sep 20–24; Chicago, Illinois. Reston: AIAA; 2004.
2. Boskovic JD, Prasanth R, Mehra RK. Retrofit fault-tolerant flight control design under control effector damage. *J Guid Control Dynam* 2007;**30**(3):703–12.
3. Edwards C, Lombaerts T, Smaili H. Fault tolerant flight control. *Lect Notes Contr Inform Sci* 2010;**399**:21–45.
4. Wang J, Li Z, Peng B. Modeling and analysis of the dissimilar redundant actuator system. *Mach Tool Hydraul* 2008;**36**(6):79–81.
5. Fu Y, Pang Y. Design and working mode analysis of dissimilar redundant actuator system. *J Beijing Univ Aeronaut Astronaut* 2012;**38**(4):432–7 [Chinese].
6. Karam W, Mare J. Force control of a rollerscrew electromechanical actuator for dynamic loading of aerospace actuators. *International conference on fluid power and motion control*. 2008 Jun 21–27; Darmstadt. Bellingham: ASME; 2008. p. 515–28.
7. Shah GH. Aerodynamic effects and modeling of damage to transport aircraft. *Proceedings of AIAA atmospheric flight mechanics conference and exhibit*. 2008 Aug 18–21; Honolulu, Hawaii. Reston: AIAA; 2008.
8. Hitachi Y. Damage-tolerant flight control system design for propulsion-controlled aircraft [dissertation]. Toronto: University of Toronto; 2009.
9. Zhao J, Jiang B, Shi P, He Z. Fault tolerant control for damaged aircraft based on sliding mode control scheme. *Int J Innovative Comput Inf Contr* 2014;**10**(1):293–302.
10. Li X, Liu HHT. A passive fault tolerant flight control for maximum allowable vertical tail damaged aircraft. *J Dynam Syst Meas Contr* 2012;**134**(3):1625–32.
11. Zhang Y, Jiang J. Active fault-tolerant control system against partial actuator failures. *IEE Proc-Contr Theory Appl* 2002;**149**(1):95–104.
12. Zhang Y, Jiang J. Integrated active fault-tolerant control using IMM approach. *IEEE Trans Aerosp Electron Syst* 2001;**37**(4):1221–35.
13. Ye D, Yang GH. Adaptive fault-tolerant tracking control against actuator faults with application to flight control. *IEEE Trans Contr Syst Technol* 2006;**14**(6):1088–96.
14. Cieslak J, Henry D, Zolghadri A, Goupil P. Development of an active fault-tolerant flight control strategy. *J Guid Contr Dynam* 2008;**31**(1):135–47.
15. Maki M, Jiang J, Hagino K. A stability guaranteed active fault-tolerant control system against actuator failures. *Int J Robust Nonlinear Contr* 2004;**14**(12):1061–77.
16. Li YX, Yang GH. Adaptive fuzzy decentralized control for a class of large-scale nonlinear systems with actuator faults and unknown dead zones. *IEEE Trans Syst Man Cybern: Syst* 2016;**99**:1–12.
17. Li YX, Yang GH. Robust fuzzy adaptive fault-tolerant control for a class of nonlinear systems with mismatched uncertainties and actuator faults. *Nonlinear Dynam* 2015;**81**(1–2):395–409.
18. Stengel RF, Huang CY. Restructurable control using proportional-integral implicit model following. *J Guid Contr Dynam* 1990;**13**(2):303–9.
19. Bodson M, Groszkiewicz JE. Multivariable adaptive algorithms for reconfigurable flight control. *IEEE Trans Contr Syst Technol* 1997;**5**(2):217–29.
20. Boškovic JD, Mehra RK. Intelligent adaptive control of a tailless advanced fighter aircraft under wing damage. *J Guid Contr Dynam* 2000;**23**(5):876–84.
21. Lavretsky E. Combined/composite model reference adaptive control. *IEEE Trans Autom Contr* 2009;**54**(11):2692–7.
22. Terra MH, Cerri JP, Ishihara JY. Optimal robust linear quadratic regulator for systems subject to uncertainties. *IEEE Trans Autom Contr* 2014;**59**(9):2586–91.
23. Chen C. On the robustness of the linear quadratic regulator via perturbation analysis of the Riccati equation [dissertation]. Dublin: Dublin City University; 2015.
24. Etkin B, Reid LD. *Dynamics of flight: Stability and control*. New York: Wiley; 1996. p. 93–114.
25. Shi C, Wang X, Wang S, Wang J, Tomovic MM. Adaptive decoupling synchronous control of dissimilar redundant actuation system for large civil aircraft. *Aerosp Sci Technol* 2015;**47**:114–24.

Wang Jun is a Ph.D. candidate at School of Automation Science and Electrical Engineering, Beihang University, Beijing, China. He received the B.S. degree in mathematics and applied mathematics from Shandong Normal University, Ji'nan, China, in 2011; and then he received the M.S. degree in mathematics from University of Science and Technology Beijing, Beijing, China, in 2014. His main research interests are fault diagnostic and fault tolerant control.

Wang Shaoping received the Ph.D., M.E. and B.E. degrees in mechatronics engineering from Beihang University, Beijing, China, in 1994, 1991 and 1988. She has been with the Automation Science and Electrical Engineering at Beihang University since 1994 and promoted to the rank of professor in 2000. Her research interests are engineering reliability, fault diagnostic, prognostic and health management, as well as active fault tolerant control.

Wang Xingjian received the Ph.D. and B.E. degrees in mechatronics engineering from Beihang University, Beijing, China, in 2012 and 2006. From 2009 to 2010, he was a visiting scholar in the School of Mechanical Engineering, Purdue University, West Lafayette, IN, U.S. He is currently with the School of Automation Science and Electrical Engineering, Beihang University, Beijing, China. His research interests are nonlinear control, active fault tolerant control, fault diagnostic and fault prognostic.

Shi Cun is a Ph.D. candidate at School of Automation Science and Electrical Engineering, Beihang University, Beijing, China. He received the B.E. degree in Mechanical Engineering from China Agricultural University, Beijing, China, in 2014. His main research interests are prognostic and health management and fault tolerant control.

Mileta M. Tomovic received the Ph.D., M.S. and B.S. degrees in mechanical engineering from University of Michigan, Massachusetts Institute of Technology, University of Belgrade, in 1991, 1981 and 1979 respectively. He has been with the mechanical engineering technology department at Purdue University from 1991 to 2008 and served as Chair of Engineering Technology Department in Old Dominion University since 2008. His research interests include design, manufacturing systems and processes, product lifecycle management, system dynamics and control.